Soft Matter: Microstructural Evolution

Visualisation of Nanostructure Evolution during Polymer Crystallisation

In the production of most textile fibres or plastics parts polymer melts are crystallised, and the developing nanostructure from crystalline domains in an amorphous matrix determines the materials properties. Engineers control temperature, composition and other parameters of the melt in order to tailor the product, but the mechanisms behind polymer crystallisation are not yet understood. We have developed a method of real-space visualisation of the domain arrangement from small-angle X-ray scattering (SAXS) patterns. *In situ* experiments were carried out at beamline **ID02**. Based on results of the new method we expect to elucidate the mechanisms which govern crystallisation and melting of polymers and their variation upon change of processing parameters.

The method combines modules from various fields of science such as beamline engineering, digital image processing, computer tomography, scattering theory and animation rendering. It extracts the information on the samples nanostructure from two-dimensional (2D) SAXS patterns with fibre symmetry using a topology $\rho(r) \in [\rho_{crys}, \rho_{amorph}]$ of phases with distinct densities. The SAXS patterns are collected by a low-noise CCD camera with fast readout that is coupled to an X-ray image intensifier (XRII–FReLoN, cycle time 7 s, exposure time between 0.1 s and 3 s). The exposure is continuously readjusted in order to keep the signal-to-noise ratio constant and high throughout the monitored process. As a result, the collected data in each image exploit the full dynamic range of the SAXS detector. 2D wide-angle X-ray scattering (WAXS) data are collected simultaneously with a second CCD camera that is coupled to a multi-channel plate (MCP-Sensicam CCD detector). Movies resulting from automatic data evaluation show an "edge-enhanced autocorrelation function" z(r) — the autocorrelation of the gradient $\nabla\rho(r)$. This "chord distribution function" (CDF) shows peaks where ever there are domain surface contacts between domains in $\rho(r)$ and its displaced ghost as a function of ghost displacement. The movies exhibit the evolution of nanostructure and demonstrate the mechanisms of polymer crystallisation.

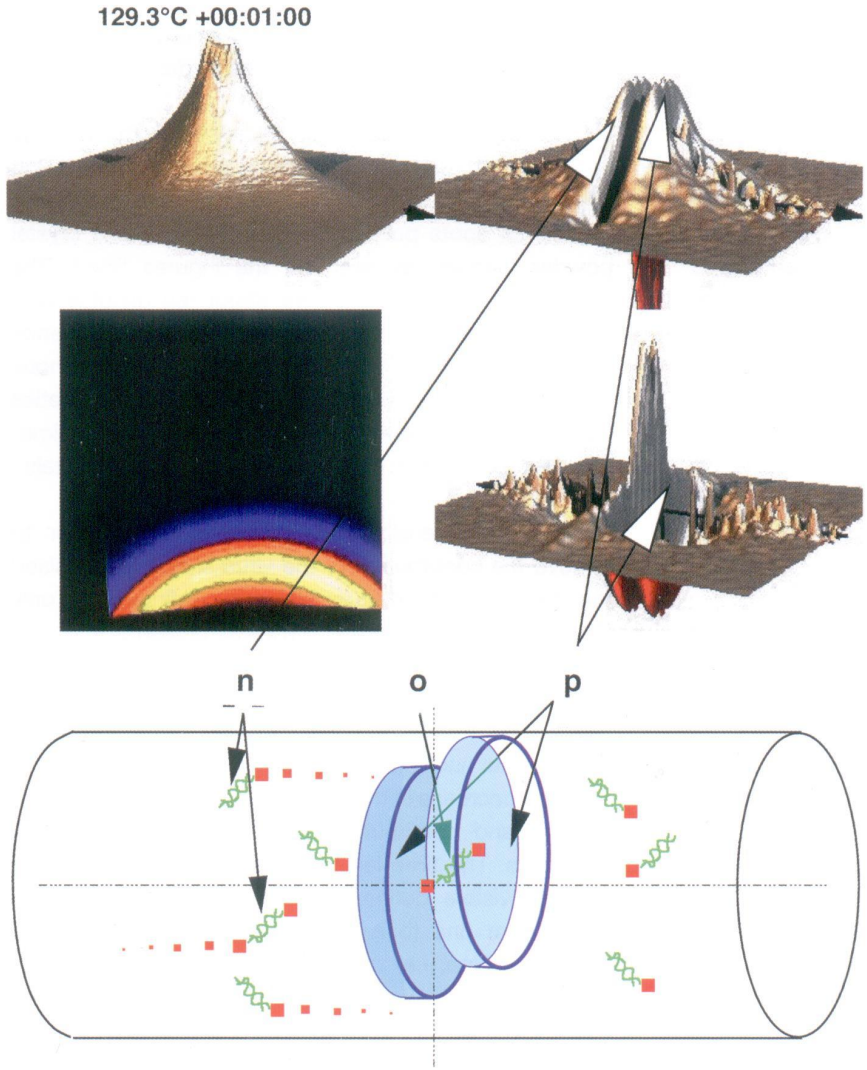

Fig. 53: Crystallisation of an oriented polyethylene melt. 1 minute after quenching to 130°C. Top: Movie frame with four panels: (left column) SAXS, WAXS; (right column) z(r), -z(r). Bottom: Sketch of the nanostructure. Off-meridional peaks (n) identified as entanglement strands and transverse shift (o) in twin-layers. Layer shape of crystals (p) from meridional peak in z(r) and self-correlation triangle in -z(r).

Figure 53 shows one movie frame representing the state 1 minute after quenching of an oriented polyethylene (PE) melt to 130°C. We observe primary, extended lamellae (stage "d" from **Figure 54,** which shows sketches of the observed phases of nanostructure evolution).

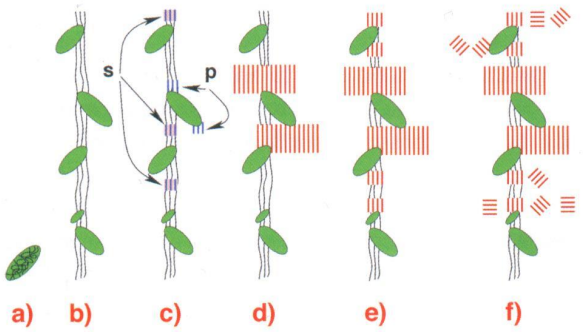

Fig. 54: Principal steps of crystallisation from a highly oriented, quiescent PE melt via a mesophase (a,b,c) coupled to primary (p) and secondary (s) crystal nuclei, extended crystalline layers (d), blocky crystals with longitudinal (e) and lateral (f) correlation.

In Figure 53 the layer character of the crystallites is demonstrated by the fact that the peaks in the CDF are extending in the direction transverse to fibre direction. The small number of peaks shows that only two layers (blue disks in the sketch) are correlated to each other. A transverse offset (p) between the members of the pair of correlated layers is induced by entities of a mesophase.

In conclusion, we found that PE crystallisation was always preceded by a mesophase structure. Based on the observed structure evolution it was suggested that its entities are entanglement-rich and disentangled regions in the melt, respectively. Extended lamellae prevail only at high crystallisation temperatures and become more perfect with time. Nevertheless, the majority of the crystallites formed during the final stages of crystallisation are small, imperfect and unoriented (*i.e.* "blocky" crystallites, Figure 54e,f). They are situated in the centre of free gaps so that correlations among crystallites are increased.

Principal Publication and Authors

N. Stribeck (a), P. Bösecke (b), R. Bayer (c), and A. Almendarez Camarillo (a) *Progr. Colloid Polym. Sci.*, (2005) in print

(a) Institute TMC, University of Hamburg (Germany)
(b) ESRF
(c) Institute of Mater. Science, GH Kassel (Germany)

Nucleation and Growth Kinetics of Brome Mosaic Virus Microcrystals

Understanding the interaction potentials that govern crystal formation is an essential step for X-ray structure determination. Brome Mosaic Virus (BMV) and polyethylene glycol (PEG) mixtures were chosen as a crystallisation model since their phase diagram presents a solid precipitated phase at high polymer concentration, known to be made of the synchronous formation of a large number of microcrystals [1]. Indeed, the addition of neutral polymers like PEG to biomacromolecular solutions results in an attractive potential (the depletion attraction) dependent upon polymer size and concentration. When the attraction increases, a fluid-fluid or fluid-solid phase separation eventually occurs.

The onset of BMV crystal nucleation and growth was observed for the first time using time-resolved X-ray scattering by the synchronisation of a fast stopped-flow mixing system (Bio-Logic) and the fast detector of **ID02**, for virus concentrations from 20 to 2.5 mg/ml and PEG concentrations down to 5% w/v. Due to the differences in molecular weights and contrasts of BMV and PEG, only the virus scattering was observed, in solution, in crystals and, possibly, in intermediary states. Twenty measurements of 50 ms each, exponentially spaced in time, were adequate to cover the process and avoid radiation damage.

Individual spots, *i.e.* Bragg peaks, arising from individual microcrystals appeared about one second after mixing (**Figures 55c-d**). After 20-60 seconds, the increasing number of spots built the diffraction rings of a crystal powder diagram as seen on the Figures 55e-f. The intensity of the rings grew for about ten minutes until there was almost no virus left in the solution. Interference rings, which would be a signature of an amorphous intermediate state, were not detected. This indicaties that only two phases were present during the time-resolved experiment: soluble viruses and microcrystals.

Dividing the intensity curves by the form factor to remove the contribution of the virus shape emphasised the structure factor (**Figure 56a**) and confirmed that only the crystallised form of the BMV was present.

The time evolution of the three parameters of Figure 56b was used to obtain the kinetic parameters of microcrystal nucleation and further growth. Both events induce a decrease in the concentration of soluble virus in solution and contribute to the increase of the peak intensities. The time lag necessary for Bragg peaks to become visible defines the onset of nucleation and varies from one to a few seconds according to the supersaturation, *i.e.* the BMV concentration. Then the diffraction peaks went on growing in essentially two steps corresponding to nucleation and crystal growth.